The Nature of the Ru−NO Bond in Ruthenium Tetraammine Nitrosyl Complexes

Giovanni F. Caramori* and Gernot Frenking*

Fachbereich Chemie, Philipps-Universität Marburg, Hans-Meerwein-Strasse, D-35032 Marburg, Germany

Received March 22, 2007

Quantum chemical calculations at the DFT level have been carried out for *trans*-$[Ru^{II}(NH_3)_4(L)NO]^q$ and *trans*-$[Ru^{II}(NH_3)_4(L)NO]^{q-1}$ complexes, where L = NH_3, Cl^-, and H_2O. The equilibrium geometries and the vibrational frequencies are reported not only for the ground state (GS) but also for light-induced metastable states MS1 and MS2. The nature of the $Ru-NO^+$ and $Ru-NO^o$ bonds has been investigated by means of the energy decomposition analysis (EDA). The nature of the Ru−NO bond has been analyzed for the three states GS, MS1, and MS2, considering two different situations: before and after one-electron reduction. The results suggest that not only the orbital term but also the ΔE_{Pauli} term is responsible for weakening of the $Ru^{II}-NO^o$ bond, the ΔE_{Pauli} term increasing in comparison with the $Ru^{II}-NO^+$ bonds, thus making the NO^o ligand more susceptible to dissociation in comparison with NO^+. Calculations of the $Ru^{III}-NO^o$ species show that in this case the bonds are mainly covalent, but the electrostatic stabilization also plays an important role. Among the orbital interactions, the π-back-donation is the most important term.

1. Introduction

The discovery of the role of nitric oxide (NO) in various physiological processes,[1,2] such as the modulation of the immune and endocrine response, cardiovascular control, regulation of blood pressure,[3] neurotransmission, induction of apoptosis, and inhibition of tumor growth,[4,5] has attracted much attention from chemists. The development of new storage-release systems to deliver NO to desired targets is a very attractive goal. In this way, the chemistry of metal nitrosyl complexes, capable of releasing NO through photochemical or chemical reduction, has experienced a considerable increase in the last decade.[6]

Among the nitrosyl complexes, ruthenium derivatives have been the focus of intense investigation due to their spectroscopic and electrochemical properties.[7,8] Moreover, these complexes exhibit high thermal stability and well-controlled NO release. Ruthenium(II) ammine nitrosyl complexes such as *trans*-$[Ru^{II}(NH_3)_4(L)NO]^{3+}$ are particularly interesting, because they are water-soluble and their synthesis and reaction pathways are well-known. In general, these complexes not only are very stable in aqueous solutions but also release NO^o through photochemical and chemical reduction. Recent studies have also shown that the release of NO^o by tetraammine nitrosyl ruthenium complexes can not only considerably increase the efficacy of both radio- and chemotherapy in hypoxic cells[9] but also block the *Trypanosoma*, *Plasmodium*, and *Leishmania* life cycle by inactivating parasite enzymes such as cysteine proteinases.[10] Complexes such as *trans*-$[Ru^{II}(NH_3)_4(L)NO]^{3+}$ constitute a very promising class of compounds, because some derivatives present redox potentials accessible to biological reducing agents such as mitochondria.[11] For example, *trans*-$[Ru^{II}(NO)(NH_3)_4(P(OEt)_3)](PF_6)_3$ is reduced by a redox potential equal to −0.10 V vs SCE. After one-electron reduction, the ion complex quickly releases NO^o (k = 0.97 s^{-1}) (eq 1).

$$\textit{trans}\text{-}[Ru^{II}(NO^+)(NH_3)_4(P(OEt)_3)]^{3+} \xrightarrow{+e^-} \textit{trans}\text{-}[Ru^{II}(NO^o)(NH_3)_4(P(OEt)_3)]^{2+}$$

$$\textit{trans}\text{-}[Ru^{II}(NO^o)(NH_3)_4(P(OEt)_3)]^{2+} + H_2O \underset{k_{+NO}}{\overset{k_{-NO}}{\rightleftharpoons}} \textit{trans}\text{-}[Ru^{II}(NH_3)_4(P(OEt)_3)(H_2O)]^{2+} + NO^o \quad (1)$$

Toledo and co-workers[12] have shown that the redox potential (NO^+/NO^o) of the tetraammine nitrosyl complexes (*trans*-$[Ru^{II}(NH_3)_4(L)NO]^{3+}$) and the lability of the NO^o ligand can be adjusted by a judicious choice of the *trans* ligand L. According to Tfouni and co-workers,[6a] an increase of the π-acidity of L implies an enhancement of the nitrosonium character of NO; that is, it is easily reduced. The influence of the *trans* ligand is also particularly relevant for determining the NO^o dissociation in *trans*-$[Ru^{II}(NH_3)_4(L)NO]^{2+}$. In this case, the rate for NO^o dissociation, depending on the different *trans* ligands L, displays

* Corresponding authors. E-mail: frenking@chemie.uni-marburg.de.

(1) Ignaro, L. J. *Pharmacol. Res.* **1989**, *6*, 651.
(2) Moncada, S.; Palmer, R. M. J.; Higgs, E. A. *Pharmacol. Rev.* **1991**, *43*, 109.
(3) Torsoni, A. S.; Barros, B. F.; Toledo, J. C., Jr.; Haun, M.; Krieger, M. H.; Tfouni, E.; Franco, D. W. *Nitric Oxide, Biol. Chem.* **2002**, *6*, 247.
(4) Culotta, E.; Koshland, D. E. *Science* **1992**, *258*, 1862.
(5) *Nitric Oxide: Biology and Pathobiology*; Ignaro, L. J., Ed.; Academic Press: San Diego, CA, 2000.
(6) (a) Tfouni, E.; Krieger, M.; McGarvey, B. R.; Franco, D. W. *Coord. Chem. Rev.* **2003**, *236*, 57, and references therein. (b) Ford, P. C.; Lorkovic, I. M. *Chem. Rev.* **2002**, *102*, 993. (c) Wang, P. G.; Xian, M.; Tang, X.; Wu, X.; Wen, Z.; Cai, T.; Janczuk, A. *Chem. Rev.* **2002**, *102*, 1091. (d) Lorkovic, I. M.; Miranda, K. M.; Lee, B.; Bernhard, S.; Schoonover, J. R.; Ford, P. C. *J. Am. Chem. Soc.* **1998**, *120*, 11674.
(7) Godwin, J. B.; Meyer, T. *J. Inorg. Chem.* **1970**, *10*, 471.
(8) Callahan, R. W.; Meyer, T. *J. Inorg. Chem.* **1976**, *16*, 574.
(9) Toledo Jr., J. C.; Lopes, L. G. F.; Alves, A. A.; Silva, L. P.; Franco, D. W. *J. Inorg. Biochem.* **2002**, *89*, 267.
(10) (a) Benini, P. G.Z.; da Silva, J. J. N.; Osakabe, A. L.; Silva, J. S. *Nitric Oxide, Biol. Chem.* **2006**, *14*, A53. (b) Venturini, G.; Salvati, L.; Muolo, M.; Colasanti, M.; Gradoni, L.; Ascenzi, P. *Biochem. Biophy. Res. Commun.* **2000**, *270* 437.
(11) Allardyce, C. S.; Dyson, P. J. *Platinum Met. Rev.* **2001**, *45*, 62.
(12) Toledo, J. C.; Silva, H. A. S.; Scarpellini, M.; Miori, V.; Camargo, A. J.; Bertotti, M.; Franco, D. W. *Eur. J. Inorg. Chem.* **2004**, 1879.

10.1021/om700271r CCC: $37.00
Publication on Web 10/13/2007

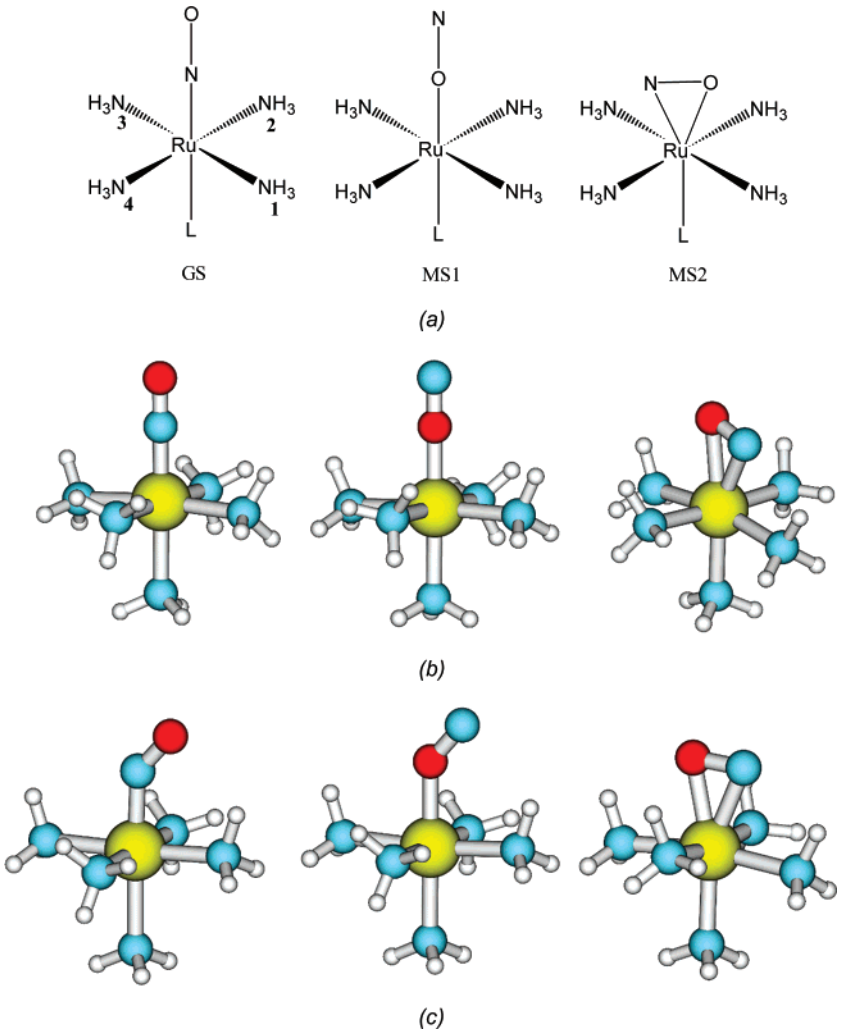

Figure 1. (a) Ground state, GS, and metastable states MS1 and MS2 of ruthenium tetraammine nitrosyl complexes. (b) Optimized structures (C_s) of ground and metastable states of $[Ru^{II}(NH_3)_5(NO)]^{3+}$ at BP86/TZ2P. (c) Optimized structures (C_s) of ground and metastable states of $[Ru^{II}(NH_3)_4L(NO)]^{q-1}$ at BP86/TZ2P.

the following trend: ImC > $P(OEt)_3$ > imN > L-hist > py > H_2O > nic ≈ 4-pic, where imC = C-bound imidazole, $P(OEt)_3$ = triethylphosphite, imN = N-bound imidazole, L-hist = L-histidine, py = pyridine, nic = nicotinamide, and 4-pic = 4-picoline.[6a]

Another important property of the nitrosyl complexes is the presence of photoinduced metastable states, MS1 and MS2, which are not electronically excited states, but rather linkage isomers in which the nitrosyl is bound through the oxygen atom (MS1) or sideways (η^2) through both oxygen and nitrogen (MS2), as shown in Figures 1a and 1b.[13,14] This kind of light-induced change was discovered in 1977, in a Mössbauer spectroscopical study of optical dispersion, by using sodium nitroprusside dehydrate, SNP, as medium.[15] Subsequently, nitrosyl complexes have been suggested as optical storage devices.[16] Following that, a differential scanning calorimetry (DSC) study, reported in 1989,[17] confirmed the presence of two metastable states of SNP. These metastable states are populated when samples are irradiated at low temperature with light of appropriate wavelength, and they are deactivated to the stable ground state isomer (GS) by red de-excitation or by thermal decay.[18] Predictably, ruthenium nitrosyl complexes also present photoinduced isomerism. The first Ru complexes for which long-lived metastable states were discovered are $K_2[RuCl_5NO]^{2-}$, $[Ru(NO_2)_4(OH)NO]^{2-}$, $[Ru(CN)_5NO]^{2-}$, and others.[19a-c]

A significant number of experimental and theoretical studies have been devoted to the chemistry of nitrosyl complexes. Among the experimental works, not only studies that investigate the structural aspects of ground or metastable states by using X-ray diffraction, FTIR spectroscopy, or DSC[13,14,20,21] but also others regarding the release of the NO group must be mentioned. Aside from that, theoretical studies that investigate electronic structure, discussing the assignment of bands in electronic spectra, vibration properties, frontier orbitals, and the excited states of ground or photoinduced metastable states, by using DFT or *ab initio* calculations must also be mentioned.[13,14,18,22a-h]

(13) Fomitchev, D. V.; Novozhilova, I.; Coppens, P. *Tetrahedron* **2000**, *56*, 6813.
(14) Kim, C.; Novozhilova, I.; Goodman, M. S.; Bagley, K. A.; Coppens, P. *Inorg. Chem.* **2000**, *39*, 5791.
(15) (a) Hauser, U.; Oestreich, V.; Rohrweck, H. D. *Z. Phys. A* **1977**, *280*, 17. (b) Hauser, U.; Oestreich, V.; Rohrweck, H. D. *Z. Phys. A* **1977**, *280*, 125.
(16) Woike, Th.; Krasser, W.; Haussühl, S. *Phys. Rev. Lett.* **1984**, *53*, 1767.
(17) Zöllner, H.; Woike, Th.; Krasser, W.; Haussühl, S. *Z. Kristallogr.* **1989**, *188*, 139.
(18) Coppens, P.; Novozhilova, I.; Kovalevsky, A. *Chem. Rev.* **2002**, *102*, 861.
(19) (a) Coppens, P. *Synchrotron Radiat. News* **1997**, *10*, 26. (b) Woike, Th.; Zöllner, H.; Krasser, W.; Haussühl, S. *Solid State Commun.* **1990**, *73*, 149. (c) Woike, Th.; Haussühl, S. *Solid State Commun.* **1993**, *86*, 333.
(20) Bottomley, F., *J. Chem. Soc., Dalton Trans.* **1974**, *15*, 1600.
(21) da Silva, S. C.; Franco, D. W. *Spectrochim. Acta A* **1999**, *55*, 1515.

Bearing in mind the importance of NO chemistry and the outstanding properties of the ruthenium ammine nitrosyl complexes,[6a] it is important to carry out a systematic study that explores the nature of the chemical bond Ru−NO in these complexes. Despite the significant number of experimental or theoretical works cited above, studies considering the nature of the chemical bonding in ruthenium ammine nitrosyl complexes are lacking in the current literature. For that reason, the aim of this work is to investigate the nature of the Ru−NO bond in the ruthenium ammine nitrosyl complexes using an energy decomposition analysis (EDA), which gives a quantitative estimate of the strength of electrostatic bonding and donor−acceptor bonding. Our study aims at providing a deep insight into the nature of the Ru−NO chemical bond and in understanding the main processes that govern the chemical behavior of the metal−ligand, Ru−NO bond. In that sense, we report a comprehensive and systematic comparison of the nature of L_n-Ru−NO bonds in tetraammine nitrosyl complexes before and after the reduction of the NO group, *trans*-$[Ru^{II}(NH_3)_4(L)NO]^q$ and *trans*-$[Ru^{II}(NH_3)_4(L)NO]^{q-1}$, where L = NH_3, H_2O, and Cl^-. Additionally, all analyses were performed not only on complexes in the GS but also on complexes in the photoinduced metastable states MS1 and MS2.

2. Methods

The geometries, harmonic frequencies, and bonding analyses have been calculated at the nonlocal DFT level of theory using the exchange functional of Becke[23] and the correlation functional of Perdew[24] (BP86). Uncontracted Slater-type orbitals (STOs) were used as basis functions for the SCF calculations.[25] Triple-ζ-quality basis sets were used, which are augmented by two sets of polarization functions: p and d functions for the hydrogen atom and d and f functions for the other atoms. This level of theory is denoted as BP86/TZ2P. An auxiliary set of s, p, d, f, and g STOs was employed to fit the molecular densities and to represent the Coulomb and exchange potentials accurately in each SCF cycle.[26] Scalar relativistic effects have been considered for the transition metals using the zero-order regular approximation (ZORA).[27] The calculations were performed by using the ADF-(2005.1) program package.[28a,b] All structures reported here have been checked to be energy minima on the potential energy surface.

The nature of the metal−ligand bond, Ru−NO, was analyzed by means of the energy decomposition analysis (EDA), implemented in the program ADF, which was originally developed by Morokuma[29] and later modified by Ziegler and Rauk.[30] EDA has been proven to be a reliable and powerful tool, improving the understanding about the nature of chemical bonding not only in main group[31] but also in transition metal compounds.[32] Since this method has been discussed in detail in the current literature,[28c,32] we will describe the involved theory only briefly. The focus of the bonding analysis is the instantaneous interaction between the two fragments of the molecule, ΔE_{int}, which is the energy difference between the molecule and its fragments in the frozen geometry of the compound. ΔE_{int} can be decomposed into three different components (eq 2),

$$\Delta E_{int} = \Delta E_{elstat} + \Delta E_{Pauli} + \Delta E_{orb} \quad (2)$$

where ΔE_{elstat} is the quasiclassical electrostatic interaction between the fragments and is calculated by considering the frozen electron-density distribution of the fragments in the geometry of the complex. The second term in eq 2, ΔE_{Pauli}, refers to the repulsive interactions between the fragments due to the fact that two electrons with the same spin cannot occupy the same region in space. It is obtained by enforcing the Kohn−Sham determinant of the orbitals of the superimposed fragments to obey the Pauli principle by antisymmetrization and renormalization. In the last step of the EDA calculation, the third term of eq 2, ΔE_{orb}, is obtained by relaxing the molecular orbitals to their optimal forms in order to yield this stabilizing interaction. This term not only incorporates Heitler−London phenomenon[33] and has additional contribution of polarization and relaxation but can also be partitioned into contributions from the orbitals that belong to different irreducible representations of the point group of the interacting system. For this reason, the EDA of complexes $[Ru^{II}(NH_3)_4(L)NO]^q$ was performed by considering fragments that possess C_s symmetry. On the other hand, for the partitioning scheme where the fragments $[Ru^{III}(NH_3)_4(L)]^q$ and NO^o are considered instead of $[Ru^{II}(NH_3)_4(L)]^{q-1}$ and NO^+, the symmetry of the interacting fragments is C_{4v} when L = Cl^- and C_{2v} when L = H_2O. This allows a convenient partitioning scheme in which the fractional occupation numbers (FON) are employed for the degenerate orbitals of both fragments.

The interaction energy, ΔE_{int}, together with the term ΔE_{prep}, which is the energy necessary to promote the fragments from their equilibrium geometry and electronic ground state to the geometry and electronic state that they acquire in the compound, can be used to calculate the bond dissociation energy (eq 3). Further details about EDA can be found in the literature.[28−32]

$$-D_e = \Delta E_{prep} + \Delta E_{int} \quad (3)$$

The figures of the molecular structures and orbitals presented in here and in the Supporting Information were obtained by using the ADFview program, available for the ADF-(2005.1) program package.[28] Figures 1a−c were drawn using the software Cs Chem Drawn Pro and Molden.

Additionally, the bonding situation of the metal−ligand and N−O bonds prior to and after one-electron reduction of the NO group was investigated using the NBO analysis,[34] in which the Wiberg bond orders[35] and the natural atomic charges were determined.

(22) (a) Gorelsky, S. I.; da Silva, S. C.; Lever, A. B. P.; Franco, D. W. *Inorg. Chim. Acta* **2000**, *300−302*, 698. (b) Gorelsky, S. I.; Lever, A. B. P.; *Int. J. Quantum Chem.* **2000**, *80*, 636. (c) Boulet, P.; Buchs, M.; Chermette, H.; DAul, C.; Gilardoni, F.; Rogemond, F.; Schläpfer, C. W.; Weber, J. *J. Phys. Chem. A* **2001**, *105*, 8991. (d) Boulet, P.; Buchs, M.; Chermette, H.; DAul, C.; Gilardoni, F.; Rogemond, F.; Schläpfer, C. W.; Weber, J. *J. Phys. Chem. A* **2001**, *105*, 8999. (e) Sizova, O. V.; Ivanova, N. V.; Sizov, V. V.; Nikolskii, A. B. *Russ. J. Gen. Chem.* **2004**, *74*, 481. (f) Sizova, O. V.; Sizov, V. V.; Baranovski, V. I. *J. Mol. Struct. (THEOCHEM)* **2004**, *683*, 97. (g) Sizova, O. V.; Lyubimova, O. O.; Sizov, V. V. *Russ. J. Gen. Chem.* **2004**, *74*, 317. (h) Sizova, O. V.; Lyubimova, O. O. *J. Mol. Struct. (THEOCHEM)* **2004**, *712*, 33.

(23) Becke, A. D. *Phys. Rev. A* **1988**, *38*, 3098.

(24) Perdew, J. P. *Phys. Rev. B* **1986**, *33*, 8822.

(25) Snijders, J. G.; Baerends, E. J.; Vernooijs, P. *At. Nucl. Data Tables* **1982**, *26*, 483.

(26) Krijn, J.; Baerends, E. J. *Fit Functions in the HFSMethod*, Internal Report (in Dutch); Vrije Universiteit, Amsterdam, 1984.

(27) (a) van Lenthe, E.; Baerends, E. J.; Snijders, J. G. *J. Chem. Phys.* **1993**, *99*, 4597. (b) van Lenthe, E.; Baerends, E. J.; Snijders, J. G. *J. Chem. Phys.* **1996**, *105*, 6505. (c) van Lenthe, E.; van Leeuwen, R.; Baerends, E. J.; Snijders, J. G. *Int. J. Quantum Chem.* **1996**, *57*, 281.

(28) (a) Bickelhaupt, F. M.; Baerends, E. J. *Rev. Comput. Chem.* **2000**, *15*, 1. (b) te Velde, G.; Bickelhaupt, F. M.; Baerends, E. J.; van Gisbergen, S. J. A.; Fonseca Guerra, C.; Snijders, J. G.; Ziegler T. *J. Comput. Chem.* **2001**, *22*, 931. (c) Lein, M.; Frenking, G. *Theory and Applications of Computational Chemistry: The First 40 Years*; Dykstra, C. E., Frenking, G., Kim, K. S., Scuseria, G. E., Eds.; Elsevier, Amsterdam, 2005; p 291.

(29) (a) Morokuma, K. *J. Chem. Phys.* **1971**, *55*, 1236. (b) Morokuma, K. *Acc. Chem. Res.* **1977**, *10*, 294.

(30) Ziegler, T., Rauk, A. *Theor. Chim. Acta* **1977**, *46*, 1.

(31) (a) Esterhuysen, C.; Frenking, G. *Theor. Chem. Acc.* **2004**, *111*, 81. (b) Kovács, A.; Esterhuysen, C.; Frenking, G. *Chem.−Eur. J.* **2005**, *11*, 1813.

(32) (a) Frenking, G.; Wichmann, K.; Fröhlich, N.; Loschen, C.; Lein, M.; Frunzke, J.; Rayón, V. M. *Coord. Chem. Rev.* **2003**, *238*−239, 55. (b) Frenking, G.; Fröhlich, N. *Chem. Rev.* **2000**, *100*, 717.

(33) Heitler, W.; London, F. *Z. Phys.* **1927**, *44*, 455.

(34) Reed, A. E.; Weinhold, F. *J. Chem. Phys.* **1983**, *78*, 4066.

(35) Wiberg, K. *Tetrahedron* **1968**, *24*, 1083.

Table 1. Calculated Vibrational Frequencies (ν(NO$^+$), cm^{-1}), Bond Lengths R (Å), Angles (deg), and Relative Energies (ΔE_{rel}) of GS, MS1, and MS2 (eV) for the Complexes *trans*-[Ru^{II}(NH$_3$)$_4$(L)NO]^q, at BP86/TZ2P (experimental values are given in *italics*)

	L = NH$_3$ (q = +3)			L = Cl$^-$ (q = +2)			L = H$_2$O (q = +3)		
	GS	MS1	MS2	GS	MS1	MS2	GS	MS1	MS2
symmetry	C_s	C_s	C_s	C_s	C_s	C_s	C_s	C_s	C_s
ν(NO)	1962	1841	1660	1891	1780	1576	1967	1835	1638
	1950[b]	*1798/1823*[b]							
R(N−O)	1.138	1.142	1.176	1.152	1.156	1.193	1.138	1.143	1.181
	1.137(1)[a]			*1.08*[b,c]			*1.142(7)*		
R(Ru−N)	1.775		1.965	1.780		1.941	1.752		1.946
	1.785(21)			*1.79(1)*			*1.715(5)*		
R(Ru−O)		1.889	2.168		1.886	2.207		1.857	2.130
R(Ru−L)	2.179	2.123	2.128	2.296	2.260	2.276	2.139	2.089	2.118
	2.094(9)			*2.355(3)*			*2.035(5)*		
R(Ru−N(1))	2.178	2.177	2.203	2.157	2.156	2.181	2.175	2.174	2.189
	2.101(2)			*2.101(8)*			*2.107(5)*		
R(Ru−N(2))	2.178	2.178	2.182	2.159	2.158	2.159	2.169	2.168	2.175
	2.101(2)			*2.109(7)*			*2.093(5)*		
R(Ru−N(3))	2.180	2.178	2.174	2.163	2.160	2.162	2.175	2.174	2.170
	2.101(2)			*2.101(8)*			*2.107(5)*		
R(Ru−N(4))	2.180	2.178	2.182	2.159	2.158	2.159	2.169	2.168	2.175
	2.101(2)			*2.109(7)*			*2.093(5)*		
∠Ru−N−O	179.1		83.2	179.9		86.0	180.0		81.9
	179.2(3)			*174.9(3)*			*178.1(5)*		
∠Ru−O−N		179.5	64.2		179.8	61.3		179.9	64.8
ΔE_{rel}	0.00	1.71	1.70	0.00	1.80	1.60	0.00	1.86	1.85

[a,b] Exptl data, refs 18, 21, and 22a. [c] Value not reliable due to disorder problems.[22a]

Furthermore, the topological analysis of the electron density[36] was carried out for complexes [Ru^{II}(NH$_3$)$_4$(L)NO]^q and [Ru^{II}(NH$_3$)$_4$(L)]$^{q-1}$.

3. Results and Discussion

3.1. Ground and Light-Induced Metastable Structures. Comparing the results of the geometry optimization of the ions *trans*-[Ru^{II}(NH$_3$)$_4$(L)NO]^q (L = NH$_3$, Cl$^-$, and H$_2$O) with C_s symmetry, and the available experimental data,[18,21,22a] it can be observed not only for GS but also for the metastable states MS1 and MS2 that the bond lengths and angles are fairly well reproduced (Table 1). In the GS and MS1 states, the ligands present a pseudo-octahedral arrangement around the metal atom and the angles Ru−N−O and Ru−O−N are close or equal to 180°, indicating the nitrosonium character in the NO ligand. The nitrosonium character of the NO ligand for all molecules *trans*-[Ru^{II}(NH$_3$)$_4$(L)NO]^q is confirmed by the reactions of these complexes with hydroxide ions, which always yield nitro compounds.[6a,37,38b] It can also be noted that neither the presence of a different axial ligand, L, nor a change in the orientation of NO affects the metal−ligand bond lengths of the equatorial ligands (numbering indicated in Figure 1a). On the other hand, the Ru−L distance is shorter in MS1 and MS2 than in GS. The distances Ru−NO are slightly larger for MS1 and MS2 than for GS. The GS and MS1 metastable states show N−O bond lengths quite similar but smaller than MS2. This tendency is confirmed by the vibrational frequencies of the NO group, which change toward smaller wavenumbers from GS to MS2. Another important observation is that when L = Cl$^-$, the N−O stretching frequencies of N−O for GS, MS1, and MS2 are smaller than the corresponding values for L = NH$_3$ or L = H$_2$O. The frequency values are a consequence of the well-established effect of the π-donor ability of the *trans* ligand, L; that is, ν_{N-O} decreases as the π-donor ability of L increases.[38] According to the relative energy results, the MS1 and MS2 states lie 1.7−1.9 and 1.6−1.9 eV above the GS state, respectively. This is in agreement with previous theoretical studies[22] and experimental results.[13,22]

Our results concerning the bonding situation are in agreement with previous theoretical studies,[22] which show that the GS structure of Ru−NO$^+$ is composed of a σ-bond Ru←:NO and two π-bonds, involving the occupied d_{xz} and d_{yz} orbitals of the metal center and the unoccupied π^*_x and π^*_y orbitals of NO. The molecular orbitals resulting from the interaction between the d_{xz} and d_{yz} orbitals of the metal center and the π^*_x and π^*_y of NO are energetically lower lying than the nonbonding HOMO, which is the d_{xy} orbital located in the equatorial plane. This behavior was observed not only for the GS ground state but also for the light-induced metastable states MS1 and MS2 (Figures S1−S3, Supporting Information).

As performed for the ions *trans*-[Ru^{II}(NH$_3$)$_4$(L)NO]^q (L = NH$_3$, Cl$^-$, and H$_2$O) with C_s symmetry, a similar analysis was carried out considering the reduced ions *trans*-[Ru^{II}(NH$_3$)$_4$(L)NO]$^{q-1}$ (L = NH$_3$, Cl$^-$, and H$_2$O) and performing unrestricted spin calculations.[39] The reduction was modeled by addition of one electron to the π^* N−O orbital, as predicted by the reduction product analysis in voltammetric experiments.[40] The experiments indicated only one monoelectronic redox process between −0.6 and 1.0 V versus SCE,[37b,38b] assigning the reduction site as the NO ligand, Ru^{II}NO$^+$/Ru^{II}NO^o. This fact was subsequently confirmed through EPR analysis,[41] which presented a large anisotropy in the g matrix, suggesting a

(36) Bader, R. F. W. *Atoms in Molecules*; Claredon Press: Oxford, 1990.

(37) (a) Lopes, L. G. F.; Wieraszko, A., El-Sherif, Y.; Clarke, M. J. *Inorg. Chim. Acta* **2001**, *312*, 15. (b) Gomes, S. S. S.; Davanzo, C. U.; Silva, S. C.; Lopes, L. G. F.; Santos, H. A.; Franco, D. W. *J. Chem. Soc., Dalton Trans.* **1998**, *37*, 601. (c) Roncaroli, F.; Ruggiero, M. E.; Franco, D. W.; Estiú, G. L.; Olabe, J. A. *Inorg. Chem.* **2002**, *41*, 5760.

(38) (a) Schreiner, A. F.; Lin, W.; Hauser, P. J.; Hopcus, E. A.; Hamm, D. J.; Gunter, J. D. *Inorg. Chem.* **1972**, *11*, 881. (b) Pell, S.; Armor, J. N. *Inorg. Chem.* **1973**, *12*, 873. (c) Borges, S. S. S.; Davanzo, C. U.; Castellano, E. E.; Z-Schpector, J.; Silva, S. C.; Franco, D. W. *Inorg. Chem.* **1998**, *37*, 2670.

(39) The open-shell fragments for the EDA can be calculated only with the ADF program by using the restricted formalism, while for the optimization of the fragments the unrestricted formalism is used. The energy differences between the restricted and unrestricted calculations are smaller than 1 kcal·mol^{-1} and are incorporated into the ΔE_{prep} values.

(40) Pipes, D. W.; Meyer, T. J. *Inorg. Chem.* **1984**, *23*, 2466.

(41) (a) Lang. L.; Davis, J.; Lopes, L. G. F.; Ferro, A. A.; Vasconcellos, L. C. G.; Prock, A.; Franco, D. W.; Tfouni, E.; Wieraszko, A.; Clarke, M. J. *Inorg. Chem.* **2000**, *39*, 2294. (b) McGravey, B. R.; Ferro, A. A.; Tfouni, E.; Bezerra, C. W.; Bagatin, I.; Franco, D.W. *Inorg. Chem.* **2000**, *39*, 3577.

Table 2. Vibrational Frequencies (ν(NO^o), cm^{-1}), Bond Lengths R (Å), Angles (deg), and Relative Energies of GS and GS1 [ΔE_{rel} (eV)] for the Complexes *trans*-[Ru^{II}(NH$_3$)$_4$(L)NO]$^{q-1}$, at BP86/TZ2P

	L = NH$_3$ ($q-1=+2$)			L = Cl$^-$ ($q-1=+1$)			L = H$_2$O ($q-1=+2$)		
	GS	MS1	MS2	GS	MS1	MS2	GS	MS1	MS2
symmetry	C_s	C_s	C_s	C_s	C_s	C_s	C_s	C_s	C_s
ν(NO)	1671	1563	1401	1591	1518	1350	1677	1549	1382
R(N−O)	1.186	1.192	1.250	1.201	1.202	1.262	1.182	1.190	1.254
R(Ru−N)	1.846		2.072	1.846		2.059	1.822		2.052
R(Ru−O)		1.990	2.082		1.981	2.096		1.951	2.054
R(Ru−L)	2.298	2.171	2.148	2.422	2.352	2.337	2.348	2.196	2.181
R(Ru−N(1))	2.157	2.160	2.178	2.138	2.137	2.155	2.157	2.158	2.172
R(Ru−N(2))	2.176	2.169	2.158	2.153	2.145	2.136	2.165	2.171	2.152
R(Ru−N(3))	2.184	2.171	2.166	2.156	2.145	2.149	2.185	2.158	2.160
R(Ru−N(4))	2.176	2.169	2.158	2.153	2.145	2.136	2.165	2.159	2.152
∠Ru−N−O	139.5		72.9	138.3		73.9	140.3		72.3
∠Ru−O−N		138.7	72.1		138.9	70.9		138.9	72.1
ΔE_{rel}	0.0	1.36	1.07	0.0	1.45	0.93	0.0	1.55	1.50

Table 3. EDA Results for *trans*-[Ru^{II}(NH$_3$)$_4$(L)NO]^q at BP86/TZ2P^a (interacting fragments are the [Ru^{II}(NH$_3$)$_4$(L)]$^{q-1}$ (f1) and NO$^+$ (f2) moieties)

	L = NH$_3$ ($q=+3$)			L = Cl$^-$ ($q=+2$)			L = H$_2$O ($q=+3$)		
	GS	MS1	MS2	GS	MS1	MS2	GS	MS1	MS2
symmetry	C_s	C_s	C_s	C_s	C_s	C_s	C_s	C_s	C_s
ΔE_{int}	35.5	76.4	65.0	−69.2	−28.2	−46.7	32.5	75.5	66.9
ΔE_{pauli}	127.7	67.6	120.1	144.2	83.1	141.2	128.7	68.6	118.3
ΔE_{elstat}	139.5	162.7	158.6	46.3	74.5	59.6	145.2	168.0	167.1
ΔE_{orb}	−231.8	−153.9	−213.7	−259.6	−185.8	−247.5	−241.4	−161.2	−218.5
$\Delta E_{(A')}$	−138.7	−91,2	−162.8	−151.3	−106.3	−180.9	−143.8	−99.6	−166.0
$\Delta E_{(A'')}$	−93.1	−62.7	−50.9	−108.3	−79.6	−66.5	−97.6	−61.6	−52.5
ΔE_σ[b]	−45.6 (19.7%)	−28.5 (18.5%)		−43.0 (16.6%)	−26.6 (14.3%)		−46.2 (19.1%)	−38.0 (23.6%)	
ΔE_π[b]	−186.2 (80.3%)	−125.4 (81.5%)		−216.6 (83.4%)	−159.2 (85.7%)		−195.2 (80.9%)	−123.2 (76.4%)	
$-D_e$	47.0	86.7	86.3	−58.7	−17.3	−24.1	42.5	86.0	89.1
ΔE_{prep}	11.5	10.3	21.3	10.5	10.9	22.6	10.0	10.5	22.2
q(f1)[c]	2.71	2.63	2.71	1.81	1.77	1.82	2.71	2.63	2.71
q(f2)	0.29	0.37	0.29	0.19	0.23	0.18	0.29	0.37	0.29

[a] Energy contributions in kcal·mol^{-1}. [b] The values in parenthese gives the percentage contribution to the total orbital interactions, ΔE_{orb}. [c] Hirshfeld charges for fragments.

Table 4. EDA Results for *trans*-[Ru^{III}(NH$_3$)$_4$(L)NO]^q at BP86/TZ2P^a (interacting fragments are the [Ru^{III}(NH$_3$)$_4$(L)]^q (f1) and NO^o (f2) moieties)

	L = NH$_3$ ($q=+3$)		L = Cl$^-$ ($q=+2$)		L = H$_2$O ($q=+3$)	
	GS	MS1	GS	MS1	GS	MS1
symmetry	C_s	C_s	C_4v	C_4v	C_2v	C_2v
ΔE_{int}	−106.1	−66.9	−94.2	−50.4	−120.6	−75.3
ΔE_{pauli}	183.6	95.0	195.2	105.1	188.0	96.8
ΔE_{elstat}[b]	−92.5 (31.9%)	−34.4 (21.2%)	−95.0 (32.8%)	−41.4 (26.6%)	−90.1 (29.2%)	−34.3 (19.9%)
ΔE_{orb}[b]	−197.2 (68.1%)	−127.5 (78.8%)	−194.3 (67.2%)	−114.1 (73.4%)	−218.5 (70.8%)	−137.8 (80.1%)
$\Delta E_{(A')}$	−128.9	−79.2				
$\Delta E_{(A'')}$	−68.3	−48.3				
$\Delta E_{(A1)}$			−49.3	−28.8	−60.5	−35.6
$\Delta E_{(A2)}$			0.0	0.0	−0.3	−0.2
$\Delta E_{(B1)}$			−0.1	−0.1	−78.7	−49.9
$\Delta E_{(B2)}$			−0.1	−0.1	−79.0	−52.2
$\Delta E_{(E1)}$			−144.8	−85.1		
ΔE_σ[c]	−60.6 (30.7%)	−30.9 (24.3%)	−49.3 (25.6%)	−28.8 (25.1%)	−60.5 (27.8%)	−35.6 (25.9%)
ΔE_π[c]	−136.6 (69.3%)	−96.6 (75.7%)	−144.8 (74.4%)	−85.5 (74.9%)	−157.7 (72.2%)	−102.1 (74.1%)
$-D_e$	−81.9	−41.9	−77.2	−35.8	−92.1	−48.8
ΔE_{prep}	24.2	25.0	17.0	14.6	28.5	26.5
q(f1)[d]	2.90	2.78	2.03	1.91	2.94	2.79
q(f2)	0.09	0.22	−0.03	0.08	0.06	0.21

[a] Energy contributions in kcal·mol^{-1}. [b] Values in parentheses give the percentage of attractive interactions $\Delta E_{elstat} + \Delta E_{orb}$. [c] The value in parentheses gives the percentage contribution to the total orbital interactions, ΔE_{orb}. [d] Hirshfeld charges for fragments.

considerable energy difference between the two π^* orbitals of NO. This indicates a bent structure of the Ru−NO bond (Ru−N−O or Ru−O−N angles are approximately 140°), as demonstrated through our calculations for the GS and MS1 states of the *trans*-[Ru^{II}(NH$_3$)$_4$(L)NO]$^{q-1}$ complexes (Table 2, Figure 1c). Due to the reduction, all N−O bonds are lengthened, which can be interpreted as a direct consequence of the decrease of the bond order, which is presented in Table 6. This finding is also confirmed by the decrease of the NO vibrational frequencies, ν_{N-O}, in comparison with ν_{N-O} values for the *trans*-[Ru^{II}(NH$_3$)$_4$(L)NO]^q complexes. After reduction, it is observed that not only the Ru−NO but also the Ru−L bond lengths for GS and MS1 increase, as a direct consequence of the Jahn−Teller effect.[42] Note that the increase of the Ru−NO and Ru−L bond lengths yields also a decrease of the bond order, as depicted in Table 6.

Additionally, as observed for Ru−NO$^+$ complexes, when L = Cl$^-$, the stretching frequencies of the N−O bond for GS,

Table 5. EDA for $[Ru^{II}(NH_3)_4(L)NO]^{q-1}$ at BP86/TZ2P[a] (interacting fragments are the $[Ru^{II}(NH_3)_4(L)]^{q-1}$ (f1) and NO^o (f2) moieties)

	L = NH_3 (q-1 = +2)			L = Cl^- (q-1 = +1)			L = H_2O (q-1 = +2)		
	GS	MS1	MS2	GS	MS1	MS2	GS	MS1	MS2
symmetry	C_s	C_s	C_s	C_s	C_s	C_s	C_s	C_s	C_s
ΔE_{int}	−63.3	−28.1	−44.5	−66.3	−31.1	−54.4	−78.1	−35.8	−48.0
ΔE_{pauli}	150.3	68.9	125.7	163.7	79.9	137.4	153.2	73.3	126.4
ΔE_{elstat}[b]	−89.9 (42.1%)	−36.2 (37.3%)	−54.1 (31.8%)	−98.0 (42.6%)	−42.7 (38.4%)	−63.7 (33.2%)	−91.4 (39.9%)	−38.2 (35.0%)	−52.3 (30.0%)
ΔE_{orb}[b]	−123.8 (57.9%)	−60.8 (62.7%)	−116.1 (68.2%)	−132.0 (57.4%)	−68.4 (61.6%)	−128.1 (66.8%)	−137.6 (60.1%)	−70.8 (65.0%)	−122.1 (70.0%)
$\Delta E_{(A')}$[c]	−76.4 (61.7%)	−38.8 (63.8%)	−106.6 (91.8%)	−75.2 (57.0%)	−37.2 (54.4%)	−118.4 (92.4%)	−86.8 (63.1%)	−46.0 (65.0%)	−112.5 (92.1%)
$\Delta E_{(A'')}$[c]	−47.4 (38.3%)	−21.9 (36.2%)	−9.5 (8.2%)	−56.8 (43.0%)	−31.2 (45.6%)	−9.7 (7.6%)	−50.8 (36.9%)	−24.9 (35.0%)	−9.6 (7.9%)
$-D_e$	−45.5	−14.2	−20.8	−50.9	−17.2	−30.3	−58.1	−22.3	−23.3
ΔE_{prep}	17.9	13.9	23.7	15.4	13.9	24.1	17.7	13.5	24.7
q(f1)[d]	2.22	2.12	2.30	1.30	1.22	1.36	2.21	2.11	2.29
q(f2)[d]	−0.22	−0.12	−0.30	−0.30	−0.22	−0.36	−0.21	−0.11	−0.29

[a] Energy values in kcal.mol^{-1}. [b] Values in parentheses give the percentage of attractive interactions $\Delta E_{elstat} + \Delta E_{orb}$. [c] The value in parentheses gives the percentage contribution to the total orbital interactions, ΔE_{orb}. [d] Hirshfeld charges for fragments.

MS1, and MS2 are smaller than the corresponding values obtained for L = NH_3 or L = H_2O, which are also caused by the π-donor ability of the *trans* ligand. It is interesting to note that for the equatorial ligands the metal−ligand bond lengths are around 2.14−2.18 Å, independent of the considered state, GS, MS1, or MS2. Moreover, the smallest values were observed for the complex with L = Cl^-, which, at the same time, showed the largest Ru−L bond lengths (Table 2).

In comparison with the complex *trans*-$[Ru^{II}(NH_3)_4(L)NO]^q$, the reduced species, *trans*-$[Ru^{II}(NH_3)_4(L)NO]^{q-1}$, has two metastable states, MS1 and MS2, which lie 1.4−1.6 and 0.9−1.5 eV above the GS state, respectively.

Not surprisingly, the structures of both ions *trans*-$[Ru^{II}(NH_3)_4(L)NO]^q$ and *trans*-$[Ru^{II}(NH_3)_4(L)NO]^{q-1}$ present geometrical parameters that reproduce quite well the chemical characteristics, as determined experimentally or predicted by earlier DFT calculations. Therefore, the obtained structures are consistent enough to be considered in the EDA, as will be discussed in the next section.

3.2. Bonding Analysis. 3.2.1. EDA of *trans*-$[Ru^{II}(NH_3)_4(L)NO]^q$ (L = NH_3, Cl^-, and H_2O). Table 3 shows the EDA results and the calculated Hirshfeld charges[43] of the NO^+ group and the remaining metal fragment in the d^6 low-spin state for the complexes $[Ru^{II}(NH_3)_4(L)]^{q-1}$, which are depicted as fragments f2 and f1, respectively (Table 3). The differences observed for ΔE_{int} are mainly due to the electrostatic and orbital contributions, while the Pauli repulsion term, ΔE_{Pauli}, independently of the nature of the trans ligand L, has the trend GS > MS2 > MS1.

As mentioned in the Methods section, EDA makes it possible to partition the orbital term into contributions that are classified according to the irreducible representations of the local symmetry point group. As the complexes have C_s symmetry, the irreducible representations are a′ and a″. In this case, the orbital interactions can be separated into σ and π. Note that for the GS and MS1 states, the total π-bonding energy is twice the a″ value because the Ru−NO^+ π bonds are nearly degenerate. This becomes obvious from Figure 2, which shows the occupied frontier orbitals of GS, MS1, and MS2 of *trans*-$[Ru^{II}(NH_3)_5NO]^q$, when the interacting fragments $[Ru^{II}(NH_3)_5]^{q-1}$ and NO^+ are considered. The energy levels and the composition of selected orbitals of the above-mentioned fragments are presented in Figures S1−S3 (Supporting information) The contribution of the second in-plane Ru−NO^+ π bond is included in the a′ orbital term. However, in the case of MS2, this separation is not possible due to the bent arrangement of the NO ligand, and therefore there is a strong mixture of σ and in-plane π interactions belonging to the irreducible representation a′, which cannot be accurately separated.

Spectroscopic studies have confirmed that the NO^+ ligand possesses a strong π-acceptor ability.[41,44] The EDA results obtained for the GS and MS1 states (Table 3) show that the metal−ligand π-orbital interactions between NO^+ and the $[Ru^{II}(NH_3)_4(L)]^{q-1}$ fragment contribute between 76.4% and 85.7% to the total ΔE_{orb} term. An increase in the π-orbital interactions is also found when the chloride ion is in the *trans* position, L = Cl^-. This confirms the strong π-donor ability of the Cl^- ion, which also promotes a decrease of the ν_{N-O} vibrational frequency. The similarities regarding the metal−

(42) (a) Jahn, H. A.; Teller, E. *Proc. R. Soc.* **1937**, *A161*, 220. (b) Jahn, H. A. *Proc. R. Soc.* **1938**, *A164*, 117.
(43) Hirshfeld, F. L.; Rzotkiewicz, S. *Mol. Phys.* **1974**, *27*, 1319.
(44) Silva, H. A. S.; Mcgarvey, B. R.; Santos, R. H. A.; Bertotti, M.; Mori, V.; Franco, D. W. *Can. J. Chem.* **2001**, *79*, 679.

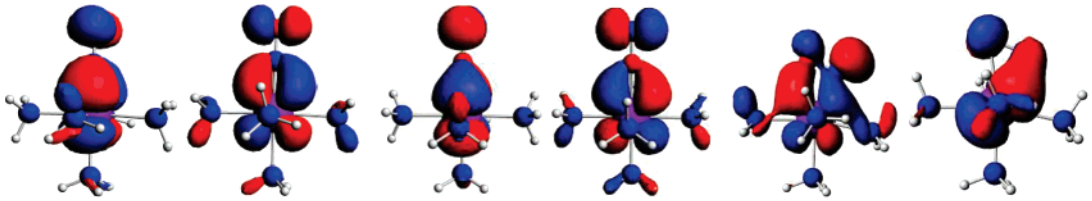

Figure 2. Orbitals depicting π-back-donation $[Ru^{II}(NH_3)_5]^{2+} \rightarrow NO^+$ of the GS, MS1, and MS2 states.

Table 6. Bond Orders and Atomic Charges, Obtained by NBO Analysis for Complexes $[Ru^{II}(NH_3)_4(L)NO]^q$ and $[Ru^{II}(NH_3)_4(L)]^{q-1}$ at BP86/TZVP, ECP = MWB28

	GS			MS1			MS2		
	bond orders	atomic charges		bond orders	atomic charges		bond orders	atomic charges	
bond	$b_{AB}{}^{w a}$	atom	q^{NPA}	$b_{AB}{}^{w}$	atom	q^{NPA}	$b_{AB}{}^{w}$	atom	q^{NPA}
				L = NH_3 (q = +3)					
Ru−N	1.278	Ru	0.596		Ru	0.682	0.983	Ru	0.640
Ru−O		N	0.353	0.655	N	0.457	0.593	N	0.314
Ru−N(1)	0.447	N(1)	−0.894	0.442	N(1)	−0.908	0.444	N(1)	−0.902
Ru−L	0.401	N(L)	−0.935	0.527	N(L)	−0.880	0.555	N(L)	−0.849
N−O	2.119	O	0.090	2.028	O	−0.076	1.931	O	−0.021
				L = Cl^- (q = +2)					
Ru−N	1.204	Ru	0.483		Ru	0.536	0.985	Ru	0.515
Ru−O		N	0.257	0.614	N	0.349	0.552	N	0.222
Ru−N(1)	0.441	N(1)	−0.882	0.437	N(1)	−0.893	0.433	N(1)	−0.865
Ru−L	0.590	Cl	−0.274	0.703	Cl	−0.225	0.744	Cl	−0.187
N−O	2.001	O	−0.008	1.955	O	−0.116	1.846	O	−0.092
				L = H_2O (q = +3)					
Ru−N	1.350	Ru	0.659		Ru	0.716	1.005	Ru	0.740
Ru−O		N	0.367	0.692	N	0.493	0.648	N	0.316
Ru−N(1)	0.454	N(1)	−0.896	0.453	N(1)	−0.908	0.454	N(1)	−0.881
Ru−L	0.276	O(L)	−0.869	0.367	O(L)	−0.827	0.369	O(L)	−0.831
N−O	2.107	O	0.097	2.039	O	−0.051	1.898	O	0.001
				L = NH_3 (q−1 = +2)					
Ru−N	1.045	Ru	0.492		Ru	0.464	0.642	Ru	0.498
Ru−O		N	0.148	0.489	N	0.193	0.480	N	0.009
Ru−N(1)	0.421	N(1)	−0.902	0.421	N(1)	−0.906	0.429	N(1)	−0.876
Ru−L	0.270	N(L)	−0.980	0.420	N(L)	−0.907	0.469	N(L)	−0.876
N−O	1.843	O	−0.159	1.807	O	−0.211	1.509	O	−0.260
				L = Cl^- (q−1 = +1)					
Ru−N	1.030	Ru	0.073		Ru	0.192	0.649	Ru	0.208
Ru−O		N	−0.143	0.490	N	−0.334	0.458	N	−0.401
Ru−N(1)	0.421	N(1)	−0.442	0.421	N(1)	−0.448	0.424	N(1)	−0.432
Ru−L	0.395	Cl	−0.316	0.550	Cl	−0.251	0.620	Cl	−0.202
N−O	1.764	O	−0.231	1.747	O	−0.205	1.479	O	−0.281
				L = H_2O (q−1 = +2)					
Ru−N	1.135	Ru	0.097		Ru	0.560	0.671	Ru	0.603
Ru−O		N	−0.093	0.566	N	0.197	0.539	N	0.018
Ru−N(1)	0.419	N(1)	−0.454	0.419	N(1)	−0.913	0.434	N(1)	−0.886
Ru−L	0.143	O(L)	−0.466	0.245	O(L)	−0.870	0.288	O(L)	−0.852
N−O	1.845	O	−0.183	1.802	O	−0.186	1.479	O	−0.240

[a] $b_{AB}{}^{(w)}$ = Wiberg bond index.

NO binding in GS and MS1 metastable states are visualized in Figures S1 and S2 (Supporting Information), which show some selected orbitals of GS and MS1 states for *trans*-$[Ru^{II}(NH_3)_5NO]^{3+}$. The qualitative similarity between GS and MS1 orbitals is obvious.

Despite the fact that it is not possible to split the large values $\Delta E_{(A')}$ for the metastable state MS2 into σ and π contributions, it is possible to assert that in bending the NO group, the overlap between the metal orbitals and the NO π* orbitals is minimized in comparison with the overlaps of the GS and MS1 states (Figure 2). In the MS2 state, the degeneracy between the orbitals involved in the π-back-donation $[Ru^{II}(NH_3)_5]^{2+} \rightarrow NO^+$ is split, as can be observed by comparing Figures S1, S2, and S3 (Supporting Information).

Table 3 shows that the energy interaction values, ΔE_{int}, for the complexes containing the neutral ligands L = NH_3 or H_2O are positive, mainly for the metastable state MS1, indicating that these complexes are thermodynamically unstable with regard to dissociation of the NO^+ group. This is due to the strong Coulomb repulsion between the ligand NO^+ and the positively charged metal fragment, as can be observed by the Hirshfeld charges of the interacting fragments, q(f1) and q(f2), which vary in the range 2.63−2.71 and 0.19−0.37, respectively. This instability is also confirmed not only by the electrostatic term, ΔE_{elstat}, which is very large when L = NH_3 or H_2O (139.5−162.7 and 145.2−167.1 kcal·mol^{-1}, respectively) but also by the positive values of $-D_e$ (47.0−86.7 and 42.5−86.0 kcal·mol^{-1}, respectively). It is interesting to note that the ΔE_{int} term is

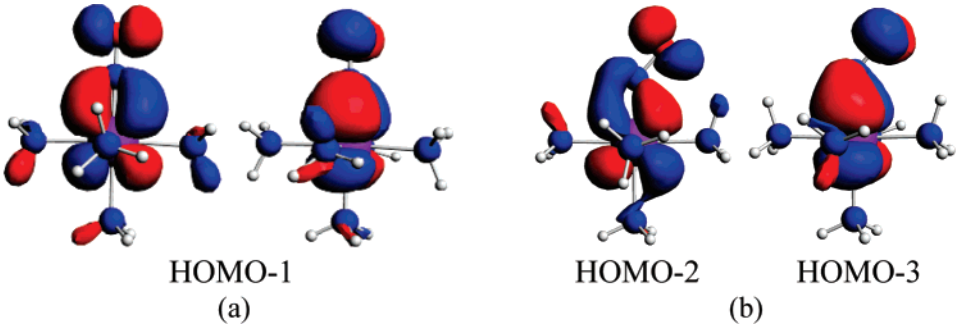

Figure 3. Molecular π-back-donation interactions in the GS states of (a) *trans*-$[Ru^{II}(NH_3)_5(NO)]^{3+}$ and (b) bent nitrosyl-metal complex *trans*-$[Ru^{II}(NH_3)_5(NO)]^{2+}$.

negative when L = Cl^-, independently of the state under consideration. This fact can be explained in terms of the ΔE_{elstat} component, which is very small when L = Cl^- (46.3−74.5 kcal·mol^{-1}) It is a direct consequence of the complex charge q, which in this case is +2, and also due to the positive charges of the interacting fragments, which are smaller when L = Cl^- than when L = NH_3 or L = H_2O. However, it was previously pointed out[45] that the absolute values of the interaction energy and the energy terms of complexes carrying different charges should not be directly compared because of the strong influence of the charges on the ΔE_{int} and ΔE_{elstat} values. The large values of ΔE_{prep}, for MS2 (21.3−22.2 kcal·mol^{-1}), in comparison with the values obtained for GS and MS1 (10.0−11.5 kcal.mol^{-1}), are related to the deformation of the fragment geometries from the equilibrium structures to the complexes, mainly in relation to the NO^+ group.

In order to explore the nature of Ru−NO chemical bonding more deeply, a new fragmentation pattern is proposed for the GS and MS1 states (Table 4). In the new scheme, $[Ru^{III}(NH_3)_4(L)]^q$ and NO^o are considered as fragments, instead of $[Ru^{II}(NH_3)_4(L)]^{q-1}$ and NO^+. To perform the EDA, the DFT-FON[46] approximation was used. The fractional occupation number FON of orbitals was employed as follows: one electron was removed from the d_π orbitals (d_{xz} and d_{yz}), which are doubly occupied and (almost) degenerate, depending on the symmetry of the compound. The unpaired electron was equally distributed to the two degenerate π* orbitals of the NO group as two half-electrons. The three remaining electrons were equally redistributed into the two d_π orbitals.

Table 4 shows that, according to the EDA, the character of the $Ru^{III}-NO^o$ bond is more covalent than electrostatic; that is, ΔE_{elstat} and ΔE_{orb} account for 19.9−32.8% and 67.2−80.1% respectively. Some differences can be noted between the electrostatic and orbital terms of the GS and MS1 states. Comparing ΔE_{elstat} and ΔE_{orb} for GS and MS1, the electrostatic character of the bond $Ru^{III}-NO^o$ is larger in GS than in MS1. The opposite behavior is observed in relation to the covalent character; ΔE_{orb} is larger in MS1 than in GS. The largest contribution to the orbital terms stems from the ΔE_π (π-backdonation) interaction, which yields 69.3−75.7% of the total covalent bonding in the complexes *trans*-$[Ru^{III}(NH_3)_4(L)NO]^q$. Yet the ΔE_σ term is still significant, contributing 24.3−30.7% of the total covalent bond. The terms ΔE_π and ΔE_σ increase and diminish, respectively, for the complexes *trans*-$[Ru^{III}(NH_3)_4(L)NO]^q$ (Table 4), in comparison with the complexes *trans*-$[Ru^{II}(NH_3)_4(L)NO]^q$ (Table 3). The ΔE_{int} values of the GS state are ∼ 40−45 kcal·mol^{-1} higher than the values of the respective MS1 state. All three contributions ΔE_{elstat}, ΔE_{Pauli}, and ΔE_{orb} are larger in the former state than in the latter. Moreover, not only the ΔE_{int} values but also D_e exhibits a similar behavior in relation to ground and metastable states. When L = Cl^-, a smaller ΔE_{int} value is observed, which can be attributed to the decrease and increase of the ΔE_{orb} and ΔE_{Pauli} terms, respectively. The EDA also indicates that the preparation energy (ΔE_{prep}) values for formation of the $Ru^{II}-NO^+$ and $Ru^{III}-NO^o$ bonds are large, particularly in the case of the metastable states MS1 and MS2. This is because the deformation of the fragment geometries from the equilibrium structures in the complexes is large. The deformation energy is especially large for the NO ligand. As will be discussed in the following sections, the presence of one electron in two degenerate π* orbitals of the NO group causes an increase of the NO bond length and thus a decrease of the NO bond order.

The EDA results show that the nature of the $Ru^{III}-NO^o$ is typically covalent, but that the electrostatic stabilization also plays a relevant role. Among the covalent interactions, the π-back-donation is the most important contribution, as already described in the literature.[6,18,22] The EDA results (ΔE_{int} and $-D_e$) suggest that the $Ru^{III}-NO^o$ bond in MS1 is more labile than in the GS state. Note that in this alternative fragmentation scheme only negative values of ΔE_{int} are obtained. This is attributed to the reduction of the electrostatic term, ΔE_{elstat}, which is negative for all complexes (Table 4).

3.2.2. EDA of *trans*-$[Ru^{II}(NH_3)_4(L)NO]^{q-1}$ (L = NH_3, Cl^-, and H_2O). According to voltammetric experiments of solutions containing ruthenium tetraammine nitrosyl complexes, just one redox process can be observed. These experiments also show that the additional electron is localized at the NO ligand, which is quickly released after electron transfer.[6a,9] For that reason, we performed the EDA for the reduced species,[39] *trans*-$[Ru^{II}(NH_3)_4(L)NO]^{q-1}$, considering as fragments NO^o and the remaining metal fragment $[Ru^{II}(NH_3)_4(L)^{q-1}$, which are depicted as f2 and f1 (Table 5).

The EDA results in Table 5 show that the $Ru^{II}-NO^o$ bonds exhibit a considerable decrease of the ΔE_{orb} term, in comparison with the values of the $Ru^{II}-NO^+$ and $Ru^{III}-NO^o$ bonds (Tables 3 and 4). This decrease of ΔE_{orb} is attributed to the reduction not only of the components $\Delta E_{(A')}$ but mainly $\Delta E_{(A'')}$. Note that the A′ component of the orbital term includes one component of the degenerate π interactions in the structures with linear RuNO moieties. Despite the fact that it is not possible to split the orbital components into σ and π interactions, the reduction of the terms $\Delta E_{(A')}$ and $\Delta E_{(A'')}$ can be attributed to the bending of the NO group. In this case, the overlap between the orbitals involved in the π-back-donation, HOMO−1−HOMO−3, is smaller than the superposition observed in the case of $Ru^{II}-$

(45) Loschen, C.; Frenking, G. *Inorg. Chem.* **2004**, *43*, 778.
(46) (a) Wang, S. G., Schwarz, W. H. E. *J. Chem. Phys.* **1996**, *105*, 4641. (b) Dunlap, B. I.; Mei, W. N. *J. Chem. Phys.* **1983**, *78*, 4997. (c) Dunlap, B. I. *Phys. Rev. A* **1984**, *29*, 2902.

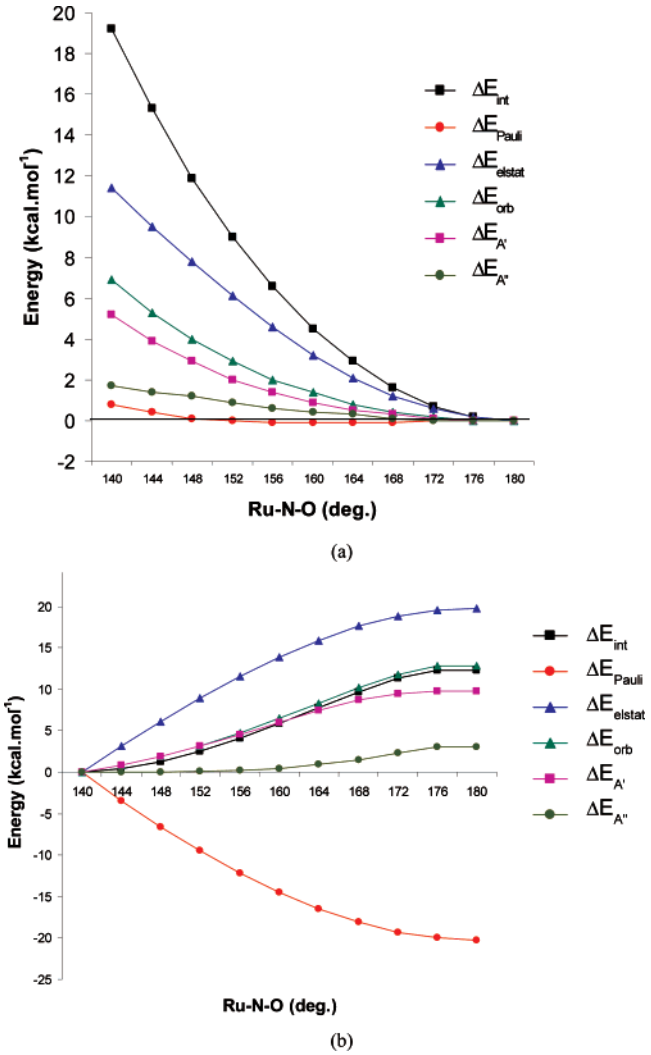

Figure 4. Relative values of EDA components obtained by bending the Ru−N−O angles of *trans*-$[Ru^{II}(NH_3)_4(Cl)NO]^{2+}$ (a) and *trans*-$[Ru^{II}(NH_3)_4(Cl)NO]^{+1}$ (b), considering structures of the GS state.

Figure 5. Contour-line diagrams of the Laplacian distribution $\nabla^2\rho(r)$ of *trans*-$[Ru^{II}(NH_3)_5NO]^{3+}$ (left) and *trans*-$[Ru^{II}(NH_3)_5NO]^{2+}$ (right) complexes in GS, MS1, and MS2 states, obtained at the level BP86/TZVP − ECP = MWB28. Dashed lines indicate charge depletion ($\nabla^2\rho(r) > 0$); solid lines indicate charge concentration ($\nabla^2\rho(r) < 0$). The solid lines connecting the atomic nuclei are the bond paths; the solid lines separating the atomic nuclei indicate the zero-flux surfaces at the molecular symmetry plane.

NO^+ bonds (Figure 3 and Figures S4−S6, Supporting Information). The HOMO (22a′ and 11a″), occupied after reduction, shows a significant antibonding character in relation to the Ru−NO^o interaction (Figures S4−S6, Supporting Information) As a consequence, a weakening of the Ru^{II}−NO^o bond is expected, making the NO^o ligand more susceptible to dissociation. Indeed, the Ru^{II}−NO^o bonds are weaker after reduction by one electron, as confirmed not only by the geometrical parameters (Tables 1 and 2), which indicate an increase of the Ru^{II}−NO^o bond lengths, but also by the bond orders, which are smaller for Ru^{II}−NO^o than for Ru^{II}−NO^+ bonds (Table 6). The largest and the smallest values of ΔE_{orb} are observed for the GS and MS1 states, respectively, while MS2 presents an intermediate value. However, not only the orbital term but also the ΔE_{Pauli} term is responsible for weakening of the Ru^{II}−NO^o, the ΔE_{Pauli} term increasing in comparison with the Ru^{II}−NO^+ bonds.

We want to point out that the MS2 state, independently of the *trans* ligand L, presents larger values of ΔE_{int} (−44.5 to −54.4 kcal·mol^{-1}) than MS1 (−28.1 to −35.8 kcal·mol^{-1}). This can be attributed to the ΔE_{orb} and ΔE_{elstat} terms, which range respectively from −60.8 to −70.8 kcal·mol^{-1} and from −36.2 to −42.7 kcal·mol^{-1} for MS1, while MS2 shows values between −116.1 and −128.1 kcal·mol^{-1} and between −52.3 and −63.7 kcal·mol^{-1}, respectively. The ΔE_{int} and $-D_e$ values suggest that the Ru^{II}−NO^o bond of the MS1 and MS2 states is more labile than that of the GS state.

As mentioned in the geometry section, the Ru−N−O angles express the nitrosonium or nitrosyl character of the NO group. Thus, for the GS and MS1 structures of the cations Ru−NO^+, the Ru−N−O angles are approximately 180°, while the neutral species Ru−NO^o show Ru−N−O angles around 140°. The following results describe the behavior of the EDA components for the GS structures with L = Cl^- when the angles Ru−N−O of Ru−NO^+ and Ru−NO^o are twisted from 180° to 140° and from 140° to 180°, with increments of 4°, respectively. In the EDA calculations the orientation of the NO fragment varies, while the structure of the fragment containing the metal was kept frozen.

According to Figure 4a, when the Ru−N−O angle of the complexes containing NO^+ changes from linear to bent, the ΔE_{int} value becomes very positive, indicating a bond instability, which mainly stems from the electrostatic and orbital components, while the Pauli term remains constant. When the Ru−N−O angles of the reduced species go from bent to linear form, not only a considerable increase of the electrostatic and orbital terms but also a decrease of the Pauli terms can be observed. A

Table 7. Bond Critical Point Properties (au)[a] of Complexes $[Ru^{II}(NH_3)_4(L)NO]^q$ and $[Ru^{II}(NH_3)_4(L)]^{q-1}$ at BP86/TZVP, ECP=MWB28

	GS			MS1			MS2		
BCP	ρ_b	$\nabla^2\rho_b$	H_b	ρ_b	$\nabla^2\rho_b$	H_b	ρ_b	$\nabla^2\rho_b$	H_b
				L = NH_3 ($q = +3$)					
Ru−N	0.174	1.060	−0.067				0.134	0.368	−0.046
Ru−O				0.112	0.922	−0.009			
Ru−$N_{(1)}$	0.083	0.289	−0.015	0.082	0.303	−0.014	0.085	0.271	−0.016
Ru−L	0.081	0.282	−0.011	0.092	0.319	−0.018	0.092	0.301	−0.018
N−O	0.606	−1.843	−1.030	0.570	−1.673	−1.118	0.554	−1.587	−0.900
				L = Cl^- ($q = +2$)					
Ru−N	0.173	1.037	−0.069				0.143	0.396	−0.053
Ru−O				0.115	0.918	−0.013			
Ru−$N_{(1)}$	0.086	0.308	−0.016	0.084	0.324	−0.015	0.086	0.287	−0.017
Ru−L	0.093	0.234	−0.026	0.100	0.248	−0.029	0.098	0.215	−0.029
N−O	0.583	−1.700	−0.953	0.550	−1.529	−1.026	0.530	−1.405	−0.814
				L = H_2O ($q = +3$)					
Ru−N	0.185	1.098	−0.076				0.139	0.381	−0.051
Ru−O				0.120	1.004	−0.012			
Ru−$N_{(1)}$	0.084	0.285	−0.016	0.083	0.301	−0.016	0.086	0.264	−0.017
Ru−L	0.069	0.380	−0.004	0.077	0.439	−0.006	0.073	0.392	−0.006
N−O	0.604	−1.804	−1.017	0.564	−1.626	−1.107	0.548	−1.538	−0.878
				L = NH_3 ($q-1 = +2$)					
Ru−N	0.165	0.673	−0.066				0.102	0.270	−0.025
Ru−O				0.096	0.615	−0.011	0.086	0.379	−0.012
Ru−$N_{(1)}$	0.076	0.330	−0.030	0.077	0.354	−0.011	0.081	0.319	−0.013
Ru−L	0.061	0.240	−0.008	0.078	0.343	−0.011	0.083	0.346	−0.013
N−O	0.535	−1.400	−0.806	0.512	−1.320	−0.820	0.452	−0.921	−0.597
				L = Cl^- (q-1 = +1)					
Ru−N	0.166	0.669	−0.068				0.106	0.283	−0.028
Ru−O				0.100	0.614	−0.013	0.083	0.377	−0.011
Ru−$N_{(1)}$	0.081	0.353	−0.013	0.081	0.383	−0.012	0.084	0.334	−0.013
Ru−L	0.069	0.210	−0.014	0.079	0.244	−0.018	0.082	0.234	−0.019
N−O	0.513	−1.267	−0.741	0.497	−1.198	−0.768	0.439	−0.838	−0.559
				L = H_2O ($q-1 = +2$)					
Ru−N	0.176	0.670	−0.078				0.108	0.275	−0.034
Ru−O				0.107	0.662	−0.015	0.394	0.082	−0.015
Ru−$N_{(1)}$	0.077	0.324	−0.012	0.080	0.362	−0.013	0.058	0.363	−0.014
Ru−L	0.042	0.223	−0.001	0.057	0.355	−0.001	−0.896	−0.034	−0.001
N−O	0.540	−1.424	−0.819	0.512	−1.310	−0.827	−0.014	−0.001	−0.585

[a] All values are in au.

false impression is created if just the ΔE_{Pauli} term is take into account, because it diminishes while the Ru−N−O angle increases, but, at the same time, a fast increase of ΔE_{elstat} is observed. For that reason, the ΔE_{int} values closely follow the trend of the ΔE_{orb} values, which can be observed by the coincident curves of ΔE_{int} and ΔE_{orb} and by the opposite behaviors of the ΔE_{Pauli} and ΔE_{elstat} terms, which basically cancel each other (Figure 4b). Therefore, the EDA results emphasize that the nitrosonium and nitrosyl groups in ruthenium tetraammine complexes assume linear and bent conformations, respectively. This is not only to minimize the electrostatic repulsion but also to acquire a conformation where the orbital interactions (mainly those involved in the π-back-donation) are maximized.

3.2.3. NBO and AIM Analyses of Complexes *trans*-$[Ru^{II}(NH_3)_4(L)NO]^q$ and *trans*-$[Ru^{II}(NH_3)_4(L)NO]^{q-1}$ (L = NH_3, Cl^-, and H_2O). In order to complement the energy decomposition analysis of the metal−ligand bonds in the ruthenium tetraamine nitrosyl complexes, before and after *trans*-$[Ru^{II}(NH_3)_4(L)NO]^q$ reduction by one electron, with a charge-decomposition analysis we carried out NBO and AIM calculations of the compounds. Table 6 shows the Wiberg[35] bond orders and the NPA charges for all complexes, in the three different states GS, MS1, and MS2. The data in Table 6 show that the bond orders for all NO bonds decrease after addition of one electron to the complex. This result is in agreement with the increase of the NO bond lengths and the decrease of the vibrational frequencies ν(NO). Note that the remaining bonds in the complexes such as Ru−L, Ru−N(1) (NH_3 equatorial), and Ru−O also have lower bond orders after reduction by one electron.

The Ru−N and Ru−O bond orders in the MS2 states indicate that prior to reduction by one electron the NO group is bonded to the metal center mainly through a nitrogen rather than a oxygen atom. The bond orders for the Ru−N bond are larger than the Ru−O values. However, after the reduction, the difference between the Ru−N and Ru−O bond orders is smaller than before addition of one electron. This result is in agreement with the AIM analysis, in which only a Ru−N bond path is observed before the reduction, while two bond paths connecting Ru−N and Ru−O are found after the reduction (Figure 5). The results agree with the calculated geometries, which show that the Ru−N and Ru−O bonds have similar bond lengths after the addition of one electron (Table 2). The NPA charges confirm the nitrosonium character of the NO^+ group before the addition of one electron, indicating that Ru and N have positive charges, while the O atoms exhibit either small positive or small negative charges.

Figure 5 shows the Laplacian of the electron density distribution of the complexes *trans*-$[Ru^{II}(NH_3)_5NO]^{3+}$ and *trans*-$[Ru^{II}(NH_3)_5NO]^{2+}$. Since the corresponding diagrams of the L = Cl^- and L = H_2O analogues are very similar, they are given in the Supporting Information (Figures S7 and S8). The Laplacian distribution around the nitrogen atoms of NH_3 groups exhibits a distortion of the region with charge concentration

$\nabla^2\rho_b < 0$, which is orientated toward the ruthenium atom. The Laplacian distribution around the NO group shows that a region of charge concentration is located mainly around the N atom. In the GS and MS1 states, the region of charge concentration around NO is slightly more distorted in the N atom after the reduction of the NO group. The AIM analysis of the metastable state MS2 does not give a Ru−O bond path before the reduction, whereas after addition of one electron, two bond paths are observed between Ru and O and between Ru and N.

The density ρ_b at the Ru−N BCP shows a decrease upon the addition of one electron at NO (Table 7). The positive values of $\nabla^2\rho_b$ are smaller after the reduction of NO, indicating a decrease of the bond polarity. A similar tendency is also observed for the MS1 and MS2 metastable states. In relation to the BCP of the Ru−O bond in MS1, the same trend is observed for ρ_b, $\nabla^2\rho_b$, and H_b; that is, after the reduction of NO group, ρ_b and $\nabla^2\rho_b$ values decrease while H_b remains constant. A considerable decrease in the covalent character of the NO bond is observed after reduction by one electron. Not only do the ρ_b values decrease but also the $\nabla^2\rho_b$ and H_b values become more positive than before the reduction of NO. Thus, the AIM analysis agrees with the conclusion that were made from the geometrical data and the EDA and NBO calculations, which show that after the reduction by one electron the NO exhibits a nitrosyl character and the Ru−NO bond is weakened.

4. Summary and Conclusion

The structures of the ground state (GS) and light-induced metastable states MS1 and MS2, obtained for *trans*-$[Ru^{II}(NH_3)_4(L)NO]^q$ and *trans*-$[Ru^{II}(NH_3)_4(L)NO]^{q-1}$ complexes, characterize the nitrosonium and nitrosyl character of the NO group, before and after one-electron reduction, respectively. The calculated vibrational frequencies reproduce very well not only the chemical characteristics of NO^+ and NO^o but also the effect of the π-acceptor ability of the *trans* ligands, L.

Complexes such as *trans*-$[Ru^{II}(NH_3)_4(L)NO]^q$ exhibit a large and positive ΔE_{elstat} term in the EDA calculations when L = NH_3 or H_2O. The EDA results also show that the π-back-donations are the most important interactions for both the GS and the MS1 and MS2 states. The EDA results also suggest that the $Ru^{III}-NO^o$ bonds are mainly covalent, but that the electrostatic stabilization also plays an important role. Among the orbital interactions, the π-back-donation is the most important term. In the case of *trans*-$[Ru^{II}(NH_3)_4(L)NO]^{q-1}$ complexes, the EDA indicates that there is a considerable reduction in the ΔE_{orb} term, mainly due to the decrease of the component $\Delta E_{(A'')}$, confirming that the overlap between the orbitals involved in the π-back-donation is smaller than the superposition observed in the case of $Ru^{II}-NO^+$ bonds. Not only the orbital term but also the ΔE_{Pauli} term is responsible for weakening of the $Ru^{II}-NO^o$, the ΔE_{Pauli} term increasing in comparison with the $Ru^{II}-NO^+$ bonds, making the NO^o ligand more susceptible to dissociation. The EDA results also emphasize that the nitrosonium and nitrosyl groups in *trans*-$[Ru^{II}(NH_3)_4(L)NO]^q$ and *trans*-$[Ru^{II}(NH_3)_4(L)NO]^{q-1}$ complexes assume linear and bent conformations, respectively, not only to minimize the electrostatic repulsion but also to acquire a conformation where the orbital interactions are maximized. The EDA results are supported by the NBO and AIM analyses.

Acknowledgment. The authors thank the computer center at HRZ Marburg for the excellent service and computational time provided. G.F.C. thanks the Conselho Nacional de Desenvolvimento Científico e Tecnológico, CNPq, Brazil, for a postdoctoral scholarship (grant 200786/2006-7). The authors also thank Andreas Krapp for helpful discussions about the manuscript.

Supporting Information Available: Cartesian coordinates, total energies (au) of the GS, MS1, and MS2 states of *trans*-$[Ru^{II}(NH_3)_5NO]^{3+}$ and *trans*-$[Ru^{II}(NH_3)_5NO]^{2+}$, contour-line diagrams of Laplacian distribution, $\nabla^2\rho(r)$, of *trans*-$[Ru^{II}(NH_3)_4(Cl)NO]^{2+}$ and *trans*-$[Ru^{II}(NH_3)_4(H_2O)NO]^{3+}$, and the calculated energy levels (au) and composition of selected orbitals of the GS state (Figures S1−S6) are available free of charge via the Internet at http://pubs.acs.org.

OM700271R